

Terahertz Multiple Access: A Deep Reinforcement Learning Controlled Multihop IRS Topology

Muhammad Shehab, *Member, IEEE*, Abdullateef Almohamad, *Member, IEEE*, Mohamed Elsayed, *Member, IEEE*, Ahmed Badawy, *Member, IEEE*, Tamer Khattab, *Senior Member, IEEE*, Nizar Zorba, *Senior Member, IEEE*, Mazen Hasna, *Senior Member, IEEE*, Daniele Trinchero.

Abstract

We investigate THz communication uplink multiple access using cascaded intelligent reflecting surfaces (IRSs) assuming correlated channels. Two independent objectives to be achieved via adjusting the phases of the cascaded IRSs: 1) maximizing the received rate of a desired user under interference from the second user and 2) maximizing the sum rate of both users. The resulting optimization problems are non-convex. For the first objective, we devise a sub-optimal analytical solution by maximizing the received power of the desired user, however, this results in an over determined system. Approximate solutions using pseudo-inverse and block-based approaches are attempted. For the second objective, a loose upperbound is derived and an exhaustive search solution is utilized. We then use deep reinforcement learning (DRL) to solve both objectives. Results reveal the suitability of DRL for such complex configurations. For the first objective, the DRL-based solution is superior to the sub-optimal mathematical methods, while for the second objective, it produces sum rates almost close to the exhaustive search. Further, the results reveal that as the correlation-coefficient increases, the sum rate of DRL increases, since it benefits from the presence of correlation in the channel to improve statistical learning.

Index Terms

DDPG, DRL, intelligent reflecting surfaces, cascaded IRS, Terahertz communication, 6G.

I. INTRODUCTION

THE sixth generation (6G) wireless communications need to provide radically modern services and bandwidth-intensive applications compared to the fifth-generation (5G) such as immersive remote presence, connected robotics; autonomous systems (CRAS), immersive extended reality (XR), and digital twin. These applications demand a $1000\times$ increase in capacity compared to 5G mobile systems [1]. To achieve these requirements and overcome the conflict between service demands and spectrum scarcity [2], there is a need to boost the current wireless spectrum bands, and migrate towards higher terahertz

M. Shehab, M. Elsayed, T. Khattab, N. Zorba, and M. Hasna are with the Electrical Engineering, Qatar University, Doha, Qatar. A. Badawy is with the Computer Science and Engineering, Qatar University, Doha, Qatar. A. Almohamad is with the Electrical and Computer Engineering, Texas A&M University Qatar, Doha, Qatar. D. Trinchero is with Dipartimento di Elettronica, Politecnico di Torino, Torino, Italy, e-mail: MuhammadShehab@ieee.org, abdullateef@ieee.org, hamid@qu.edu.qa, badawy@qu.edu.qa, tkhattab@ieee.org, nizarz@qu.edu.qa, hasna@qu.edu.qa, and daniele.trinchero@polito.it. This research work was made possible by grant number AICC03-0530-200033 from the Qatar National Research Fund (QNRF). Statements made herein are the sole responsibility of the authors.

(THz) frequency bands which range from 0.1 THz to 10 THz. These frequencies are considered a key element in 6G wireless communications because they possibly support considerable capacities and data rates. However, high-frequency values lead to severe path attenuation, high propagation losses, and sporadic wireless links. Further, these values produce very small wavelength (λ) values, which in turn results in very short communication distances and increases the susceptibility to molecular absorption and blockage [1]. To improve the received signal power, and achievable data rate, this paper investigates the intelligent reflecting surface (IRS) as an emerging technology and promising solution [3]. IRS manipulates the incident electromagnetic waves and adjusts the phase shifts of the semi-passive reflecting elements in a programmable behavior to yield a smart radio environment and enhance the data rate in an energy-efficient and cost-effective manner [4].

Many recent studies examined IRS deployment in THz communications to inspect the power of IRS to improve the coverage and achievable data rate [5] - [11]. For instance, the authors in [5] studied the scenario of IRS-assisted multi-hop multi-pair unicast network, where multiple sources are communicating with multiple destinations. They proposed distributed multiple IRSs controls for a multi-hop interference channel with the purpose of maximizing the achievable rate. A multi-IRS assisted massive multiple-input multiple-output system was studied [6] to increase the minimum received signal power, where a base station (BS) equipped with multi-antenna transmits independent signals to a group of remote users equipped with single-antenna, and a cascaded line-of-sight (LOS) communication links are established among the BS and users by using the cooperative signal reflections of various IRSs groups. In [7] the authors examined the performance of the rate achieved for a decode-and-forward (DF) relaying assisted multi-IRS system, where a single source is communicating with a single destination (user) with the objective of obtaining the optimal IRSs configuration, number of IRSs, and number of IRS reflecting elements that maximize the ergodic rate. Further, in [8] the authors considered a multi-hop IRS-assisted multi-user downlink communication scenario, where the BS is communicating to K users with the scope of maximizing the sum rate by jointly optimizing the beamforming at the BS, and the multiple IRS phase shift reflection matrices. Moreover, in [9], the authors investigated the scenario of an uplink multi-hop IRS communication system where multi-users (sources) are communicating with a single destination. Their scope was to extend the link range in THz communications and maximize the power at the receiver. They proposed a cascaded passive IRS THz system to overcome the high propagation losses caused by the absorption in the air molecules.

To this end, the aforementioned research papers [5] - [9] adopted mathematical techniques to solve their optimization problem. Unlike these studies, the research papers in [10] and [11] utilized the DRL algorithm to solve the non-convex optimization problem. The authors proposed a hybrid beamforming scheme for the cascaded IRS-aided networks to enhance the coverage of the THz communication links. They investigated the joint design of the analog beamforming at the IRSs and the digital beamforming at the BS to overcome the propagation loss in THz downlink broadcast system, which is a single source to a multi-destination (multi-user) scenario.

A. Contributions

To extend the range of the THz links and compensate for the losses at such a high operating frequency range, we adopt multi-hop IRSs (also referred to as cascaded IRSs) as the core component in our system model. Since, this is typical environment for users using THz links where the coverage is small, then we only consider small areas where several users are not expected.

Thus, we formulate an optimization problem under the assumption of a two-user system, where the objective is to find the optimum phase shifts of the multi-hop IRS's element in order to maximize the received rate for any specific user, and the sum rate for both users. The major challenge in our scheme lies in the non-convexity of the objective function due to the constant modulus constraints of the reflecting IRS elements, non-linear constraints, and computationally intractable multi-hop links. In general, the optimal solution to this NP-hard problem is unknown, and it is difficult to derive an analytical solution using traditional mathematical methods, and the exhaustive search is not practical for large-scale communication systems [10], [11]. In addition, solving the problem of the received rate maximization leads to an over-determined system. To tackle this, we exploit a Deep Deterministic Policy Gradient (DDPG)-based algorithm, which is a DRL method, to obtain feasible solutions.

To the best of our knowledge, none of the existing research papers in the literature leveraged the DRL method to solve the over-determined system of equations for the uplink cascaded IRS multiple access scenario. In this paper, we address the above-mentioned gap in the literature by employing DRL- in particular, DDPG, to jointly optimize the phase shifts of each IRS in the cascaded IRS system taking into consideration the case of the spatially correlated channel [12] between IRS₁ and IRS₂, to achieve two main objectives: a) maximizing the rate for any specific user, and b) maximizing the sum rate for both users.

We detail our contributions below against our two main objectives under the consideration of multi-hop IRSs and multiple access systems operating in the THz range:

- Our first objective is to maximize the rate for any specific user under the assumption that the second user is considered as interference. For this objective:
 - We formulate the cascaded IRS phase shift optimization problem that includes IRS₁ and IRS₂ phases as a closed form, and we prove that it is non-convex and mathematically intractable.
 - Further, to overcome this, we propose two sub-optimal solutions, where our objective is to find the optimal phases of the IRS₁ and IRS₂ elements that maximize the received power of the desired user. We show that when solving for the optimized phase shifts that maximize the received power of the desired user, the system is over-determined and therefore, we propose two solutions for this problem through the use of pseudo-inverse and block solutions.
 - Moreover, we design a DDPG algorithm to find the optimum phases that maximize the rate of the desired user.
- Our second objective is to maximize the sum rate of two users, For this objective:
 - We provide analytical analysis for the problem in the case of cascaded IRSs.
 - We design a DDPG algorithm to obtain the optimum phase shifts of the cascaded IRSs that maximize the received sum rate.
- We simulate our proposed solutions and compare the obtained results to those obtained through the exhaustive search algorithm and through randomly generated phase shifts.

B. Paper organization

The remainder of this research paper is structured as follows; section II describes the system and channel model for the multi-hop IRS scenario. Section III presents the problem formulation for maximizing the rate of the desired user operating

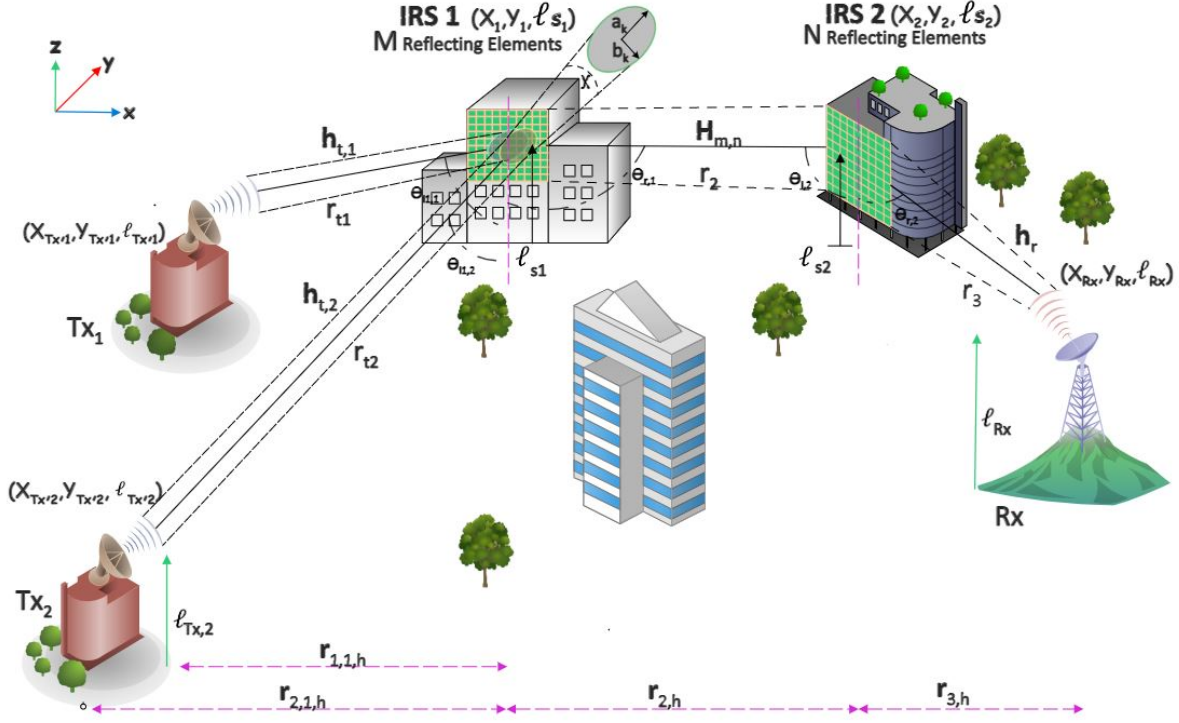


Figure 1: Cascaded IRS system model.

under interference, and Section IV discusses sum rate maximization problem for both users. Thus, it discusses the end-to-end sum rate derivation in the cascaded IRS scenario. Section V introduces the proposed solution using DDPG for the cascaded IRS phase control. The simulation results are discussed in section VI, and section VII concludes the paper.

Notation: For more convenience, frequent symbols and parameters along with their description are illustrated in Table 1.

II. SYSTEM AND CHANNEL MODEL

In our system model, we assume that we have two single-antenna users operating in an uplink multi-hop IRS communication system as shown in Fig. 1, where the operating frequency is within the THz range. The two users are equipped with highly directional parabolic antennas and transmit the signal focused to the center of IRS₁. The antenna diameter for each transmitter is D_t and for the receiver is D_r . The distances between the two users and IRS₁, IRS₁ and IRS₂, and between IRS₂ and R_x , are denoted as r_{tk} , r_2 , and r_3 respectively. The horizontal distances between the transmitters and the center of IRS₁, the center of IRS₁ and the center of IRS₂, IRS₂, and the receiver R_x are denoted as $r_{k,1,h}$, $r_{2,h}$, and $r_{3,h}$ respectively. The incident and reflected angles with respect to the center of the illuminated areas at IRS₁ and IRS₂ are represented as $\theta_{i1,1}$, $\theta_{i2,1}$, $\theta_{r,1}$, $\theta_{i,2}$, and $\theta_{r,2}$ respectively. The heights of the two transmitters, IRS₁, IRS₂, and the receiver R_x are denoted as $\ell_{Tx,1}$, $\ell_{Tx,2}$, ℓ_{s1} , ℓ_{s2} , and ℓ_{Rx} respectively. The IRSs act as beamformers that focus the incident signal at a particular reflection direction by modifying the phases of the reflecting units (RUs). The number of RUs in IRS₁ is $M = M_x \times M_y$ and the number of RUs in IRS₂ is $N = N_x \times N_y$.

Table 1: List of frequently used parameters and symbols.

Parameters and Symbols	Description
x_k	Transmitted signal for each user k
y_k	Received signal for each user k
z_k	Signal for each user k
P_t	Transmit power for each user
λ	Wavelength
\mathbf{h}_r	Channel between IRS2 and the receiver
$\mathbf{H}_{m,n}$	Channel between IRS ₁ and IRS ₂
$\mathbf{h}_{t,k}$	Channel between each user k and IRS ₁
n_0	AWGN in linear scale
K_1, K_2	Rician Factor for the transmitter channel and receiver channel
\mathbf{R}	Covariance Matrix
Φ_M, Φ_N	Phase shift reflection matrix for IRS ₁ and IRS ₂ , respectively
ϕ_m, ϕ_n	Phase shift of IRS ₁ reflecting element m and IRS ₂ reflecting element n , respectively
η_m	Phase shift of m^{th} IRS ₁ reflecting element
ψ_n	Phase shift of n^{th} IRS ₂ reflecting element
D_t, D_r	Antenna diameters for each T_{x_k} and R_x , respectively
r_{tk}, r_2, r_3	Distance between: each user k and IRS ₁ , IRS ₁ and IRS ₂ , and IRS ₂ and R_x , respectively
$r_{k,1,h}, r_{2,h}, r_{3,h}$	Horizontal distance between: user k and center of IRS ₁ , centers of IRS ₁ and IRS ₂ , and center of IRS ₂ and R_x , respectively
$\theta_{ik,1}$	Incident angle from user k w.r.t. the center of the illuminated area at IRS ₁
$\theta_{r,1}$	Reflected angle w.r.t. the center of the illuminated area at IRS ₁
$\theta_{i,2}$	Incident angle from IRS ₁ w.r.t. the center of the illuminated area at IRS ₂
$\theta_{r,2}$	Reflected angle w.r.t. the center of the illuminated area at IRS ₂
$\ell_{Tx,k}, \ell_{Rx}, \ell_{s1}, \ell_{s2}$	The height of the T_{x_k} , R_x , IRS ₁ and IRS ₂ , respectively
M, N	Number of reflecting elements for IRS ₁ and IRS ₂ respectively
$[\mathbf{R}]_{m,n}$	Covariance matrix obtained based on the exponential spatial correlation model
$\rho^{ m-n }$	Correlation-coefficient among the adjacent RUs
Ω_k	Phase shifts corresponding to signal traveled from user k to IRS ₁
Ω_3	Phase shift corresponding to signal traveled from IRS2 to R_x
o	Angle measured from the broadside of the antenna
$G_t(o), G_r(o)$	Gains for the users' and receiver antennas respectively
e_t, e_r	Aperture Efficiencies for the T_{x_k} and R_x
$L_{\tau,k}$	Total losses and gains on the path between each T_{x_k} and the R_x
$L_{FSPL,\tau,k}$	Total FSPL for T_{x_k}
$L_{abs,\tau,k}$	Total absorption loss for T_{x_k}
$G_{t,k} G_r$	T_{x_k} , and R_x antenna gains
$G(\theta_{i1,k}), (\theta_{r,1})$	Gain of IRS ₁ RU from the incident and reflection angles
$P_{r,m}$	The power reflected from the m_{th} RU of IRS ₁
$P_{r,mn}$	The power reflected from the n_{th} RU of IRS2 because of being illuminated by the signal reflected by the m_{th} RU of IRS ₁
$P_{rx,mn}$	The received captured power at the R_x
P_{Rx_k}	The total received power for user k at the receiver (R_x)
α_m	The reflection coefficient of the m^{th} RU of IRS ₁
α_n	The reflection coefficient of the n^{th} RU of IRS ₂
φ_{tkm}	The phase for the transmitter channel for user k and m^{th} RU
φ_{mn}	The phase for the $\mathbf{h}_{m,n}$ channel for m^{th} and n^{th} RU
φ_{rn}	The phase for the receiver channel for n^{th} RU
γ_k	The received SINR for the T_{x_k} at the R_x
$R_k,$	The data rate for user k
R_{sum}	and in practical and in practical
Ξ	Phase search steps

The transmitted signal for each user k , where $k \in 1, 2$, is represented by the following equation:

$$x_k = \sqrt{P_t} z_k, \quad (1)$$

where z_k represents the signal for user k with unit power (i.e., $\mathbb{E}[|z_k|^2] = 1$, $\mathbb{E}[\cdot]$ denotes the expectation), and P_t represents the transmit power for each user.

Thus, the received signal for each user k is denoted by:

$$\begin{aligned} y_k &= \mathbf{h}_r^H \Phi_N \mathbf{H}_{m,n}^H \Phi_M \mathbf{h}_{t,k}^H x_k + n_0, \\ y_k &= \mathbf{h}_r^H \Phi_N \mathbf{H}_{m,n}^H \Phi_M \mathbf{h}_{t,k}^H \sqrt{P_t} z_k + n_0, \end{aligned} \quad (2)$$

where $\mathbf{h}_{t,k} \in \mathbb{C}^{1 \times M}$ is the channel between each user k and IRS₁, $\mathbf{H}_{m,n} \in \mathbb{C}^{M \times N}$ is the channel between IRS₁ and IRS₂, $\mathbf{h}_r \in \mathbb{C}^{N \times 1}$ is the channel between IRS₂ and the receiver, $\Phi_M = \text{diag}(e^{-j\eta_1}, e^{-j\eta_2}, \dots, e^{-j\eta_M})$ and $\Phi_N = \text{diag}(e^{-j\psi_1}, e^{-j\psi_2}, \dots, e^{-j\psi_N})$ are the phase shift reflection matrices for IRS₁ and IRS₂ respectively that satisfy the constant modulus constraint $|\phi_m|^2 = |e^{-j\eta_m}|^2 = 1$, $\forall m \in \{1, 2, \dots, M\}$ and $|\phi_n|^2 = |e^{-j\psi_n}|^2 = 1$, $\forall n \in \{1, 2, \dots, N\}$, and $\text{diag}(\cdot)$ denotes the diagonal matrix. Moreover, the phase shifts of the m^{th} and n^{th} reflecting elements are represented by η_m and ψ_n , where η_m and ψ_n values are between 0 and 2π , and the noise $n_0 \sim \mathcal{CN}(0, \sigma^2)$ represents the AWGN for each user in linear scale.

Moreover, the deterministic phase shifts corresponding to the traveled distances of the signals from each user k over the first hop, and the IRS₂- R_X link over the third hop are represented as follows:

$$\begin{aligned} \Omega_k &= 2\pi r_{t_k} / \lambda, \\ \Omega_3 &= 2\pi r_3 / \lambda. \end{aligned} \quad (3)$$

where λ is the wavelength, and it is equal to c/f where c is the speed of light equal to 3×10^8 m/s and f is the frequency measured in Hertz (Hz).

The transmitter and receiver channels $\mathbf{h}_{t,k}$, and \mathbf{h}_r follow the Rician fading model [11], [13]:

$$\mathbf{h}_{t,k} = \sqrt{\frac{K_1}{K_1 + 1}} \bar{\mathbf{h}}_{t,k} + \sqrt{\frac{1}{K_1 + 1}} \tilde{\mathbf{h}}_{t,k}, \quad (4)$$

$$\mathbf{h}_r = \sqrt{\frac{K_2}{K_2 + 1}} \bar{\mathbf{h}}_r + \sqrt{\frac{1}{K_2 + 1}} \tilde{\mathbf{h}}_r, \quad (5)$$

where K_1 is the rician factor of $\mathbf{h}_{t,k}$. $\bar{\mathbf{h}}_{t,k} \in \mathbb{C}^{1 \times M}$, and $\tilde{\mathbf{h}}_{t,k} \in \mathbb{C}^{1 \times M}$ are the LOS component, and non-LOS (NLOS)

component respectively. Similarly, K_2 is the rician factor of \mathbf{h}_r , $\bar{\mathbf{h}}_r \in C^{N \times 1}$ and $\tilde{\mathbf{h}}_r \in C^{N \times 1}$ are the LOS component and NLOS component respectively. The channel between IRS₁ and IRS₂, $\mathbf{H}_{m,n} \sim \mathcal{CN}(0, \mathbf{R})$, follows the spatially correlated Rayleigh fading channel model, where \mathbf{R} is the covariance matrix obtained based on the exponential spatial correlation model. It is controlled using the parameter $\rho \in [0, 1]$ which represents the correlation-coefficient among the adjacent RUs, and it is expressed as:

$$[\mathbf{R}]_{m,n} = \rho^{|m-n|} e^{j(m-n)\theta_{i,2}} \quad (6)$$

where $\theta_{i,2}$ is the angle of arrival between IRS₁ and IRS₂. High values of ρ , result in high correlation among \mathbf{H}_{mn} elements, and in cases where ρ is less than 1 (i.e. not equal to 1), the significant correlations are between adjacent RUs only, with considerably low correlation at large distances. Further, we assume that the channels $\mathbf{h}_{t,k}$, and \mathbf{h}_r are perfectly known for all the transmitters and the receiver. Even-though the channel estimation, and finding out the channel state information (CSI) [14] is a challenging task for IRS-based communication networks, some studies proposed significant methods for obtaining CSIs. The authors, in [15] proposed an efficient channel estimation algorithm for a double IRS-based assisted multi-user MIMO communication system to obtain the cascaded CSI. In [16], the authors conducted a comprehensive survey on channel estimation for IRS-assisted wireless communications focused on solutions that tackle practical design problems. The study in [17] proposed a framework for IRS channel estimation where a small number of IRS elements are capable of processing the received signal to facilitate channel estimation. Thus, the IRS estimates the channel between itself and the BS, and between itself and the users based on the pilot signals received by the IRS semi-passive elements utilizing compressed sensing methods.

Further, the gains for the users' and receiver antennas $G_t(o)$ and $G_r(o)$ are expressed as:

$$G_{\mathcal{X},k}(o) = 4e_{\mathcal{X}} \frac{J_1\left(\frac{\pi D_{\mathcal{X}} \sin(o)}{\lambda}\right)}{\sin(o)}, \mathcal{X} \in \{t, r\}. \quad (7)$$

where $J_1(\cdot)$ is the first-order Bessel function of the first kind, $D_{\mathcal{X}}$ is the diameter of the antenna, and $\mathcal{X} \in \{t, r\}$ represents Tx or Rx antennas, respectively. The angle measured from the broadside of the antenna is represented as o [18].

Thus, the maximum gain is for $o = 0$ and it is denoted as:

$$G_{\mathcal{X},k}(o) = e_{\mathcal{X}} \left(\frac{\pi D_{\mathcal{X}}}{\lambda}\right)^2, \mathcal{X} \in \{t, r\}. \quad (8)$$

where e_t and e_r represents the aperture efficiencies for the T_x and R_x respectively. Further, the gain of every RU is expressed as [18]

$$G(\theta_{i1,k}) = 4 \cos(\theta_{i1,k}), \quad 0 \leq \theta_{i1,k} \leq \pi/2, \quad (9)$$

where $\theta_{i1,k}$ is the angle of incidence from user k to IRS₁. [18].

The total losses and gains on the path between each T_{x_k} and the R_x are denoted by $L_{\tau,k}$. This includes the antenna gains, free space path loss (FSPL), and THz absorption loss (AS).

$$L_{\tau,k} = L_{FSPL,\tau,k} L_{abs,\tau,k}, \quad (10)$$

where $L_{abs,\tau,k}$ represents the total THz absorption losses for each T_{x_k} . These THz losses are obtained under standard atmospheric conditions utilizing the simplified model suggested in [19], and $L_{FSPL,\tau,k}$ represents the total FSPL for each T_{x_k} , and it is denoted as:

$$L_{FSPL,\tau,k} = L_{FSPL,k} L_{FSPL,r}. \quad (11)$$

$L_{FSPL,k}$ for the signal reflected from IRS₁ towards IRS₂ is represented as

$$L_{FSPL,k} = \frac{\left(\frac{\lambda}{4\pi}\right)^2 G_{t,k} G_{\theta_{i1,k}} G_{\theta_{r,1}}}{r_{t_k}^2}, \quad (12)$$

and $L_{FSPL,r}$ between IRS₁ and the receiver is expressed as

$$L_{FSPL,r} = \frac{\left(\frac{\lambda}{4\pi}\right)^4 G_{\theta_{i,2}} G_{\theta_{r,2}} G_r}{r_2^2 r_3^2}. \quad (13)$$

Thus, the total FSPL for each T_{x_k} is expressed as

$$L_{FSPL,\tau,k} = \left(\frac{\lambda}{4\pi}\right)^6 \frac{G_{t,k} G(\theta_{i1,k}) G(\theta_{r,1}) G(\theta_{i,2}) G(\theta_{r,2}) G_r}{r_{t_k}^2 r_2^2 r_3^2}. \quad (14)$$

III. MAXIMIZING THE RATE OF A DESIRED USER UNDER INTERFERENCE

In this section, we provide the analytical derivations of the first objective, which is maximizing the rate of a desired user, while the other user is considered an interferer. Our objective is to find the optimum phases of the cascaded IRSs that maximize the received rate of the desired user. We will show that the rate maximization problem is non-convex and finding a closed-form expression of the IRS phases is mathematically intractable. Then we propose sub-optimal solution to the problem through maximizing the received power of the desired user. In addition, we propose a DDPG algorithm that maximizes rate of a the desired user.

A. Rate of the Desired User Under Interference

The analytical form of the rate of the desired user under the interference scenario can be written as

$$R_k = \log_2(1 + \gamma_k), \quad (15)$$

where γ_k is the signal to interference plus noise ratio (SINR) of user k . The SINR, γ_k , can be written as

$$\gamma_k = \frac{P_{Rx}^k}{\sum_{\substack{i=1 \\ i \neq k}}^K P_{Rx}^i + \sigma^2}, \quad (16)$$

where P_{Rx}^k is the received power of user k and σ^2 is the noise variance. In the following, we provide the analytical derivations of P_{Rx}^k .

1) *User's Received Power (P_{Rx}^k):* In our scenario, both users are transmitting at IRS₁, covering all IRS₁ elements from various angles and distances. The power reflected from the m^{th} RU of IRS₁ can be written as in [18] without including the absorption losses calculation. $L_{abs,\tau,k}$ is included in $L_{\tau,k}$ in the expression for the total received power.

$$P_{r,m}^k = \left(\frac{\lambda}{4\pi}\right)^2 \frac{G_{t,k}G(\theta_{i1,k})G(\theta_{r,1})}{r_{tk}^2} \times |h_{t,km}|^2 |\alpha_m|^2 P_t, \quad (17)$$

where $\alpha_m = \alpha e^{-j\eta_m}$ designates the reflection coefficient of the m^{th} RU of IRS₁; $G_{t,k}$ represents the T_x antenna gain of user k ; $G(\theta_{i1,k})$ and $G(\theta_{r,1})$ represent the gain of RU from the incident and reflection angles, respectively; and $r_{t,k}$ is the distance between T_{x_k} and RU m . Similarly, the reflected power from the n^{th} RU of IRS₂ because of being illuminated by the signal reflected by the m^{th} RU of IRS₁ is

$$P_{r,mn}^k = \left(\frac{\lambda}{4\pi}\right)^4 \frac{G_{t,k}G(\theta_{i1,k})G(\theta_{r,1})G(\theta_{i,2})G(\theta_{r,2})}{r_{tk}^2 r_2^2} \times |h_{t,km}|^2 |\alpha_m|^2 |H_{mn}|^2 |\alpha_n|^2 P_t, \quad (18)$$

where $\alpha_n = \alpha e^{-j\psi_n}$ designates the reflection coefficient of the n^{th} RU of IRS₂, H_{mn} represents the (m,n) element of the IRS₁-IRS₂ channel matrix \mathbf{H} . Finally, the received captured power at the R_x through channel H_{mn} can be written as follows

$$P_{rx,mn}^k = \left(\frac{\lambda}{4\pi}\right)^2 \frac{P_{r,mn}^k}{r_3^2} G_r |h_{rn}|^2. \quad (19)$$

$$P_{rx,mn}^k = \left(\frac{\lambda}{4\pi}\right)^6 \frac{G_{t,k}G(\theta_{i1,k})G(\theta_{r,1})G(\theta_{i,2})G(\theta_{r,2})G_r}{r_{tk}^2 r_2^2 r_3^2} \times |h_{t,km}|^2 |\alpha_m|^2 |H_{mn}|^2 |\alpha_n|^2 |h_{rn}|^2 P_t, \quad (20)$$

and the total received power for user k at the receiver (R_x) is expressed as [18]

$$P_{Rx}^k = |\sqrt{L_{\tau,k}} \sum_{m=1}^M \sum_{n=1}^N |h_{t,km}| |\alpha_m| |H_{mn}| |\alpha_n| |h_{rn}| e^{-j(\varphi_{t_{km}} + \eta_m + \varphi_{mn} + \psi_n + \varphi_{rn} + \Omega_k + \Omega_3))}|^2 P_t, \quad (21)$$

where $\varphi_{t_{km}}$ is the phase for the transmitter channel for user k and m^{th} RU, φ_{mn} is the phase for the $\mathbf{h}_{m,n}$ channel for m^{th} and n^{th} RU, φ_{rn} is the phase for the receiver channel for n^{th} RU, $|\alpha_n|$ and $|\alpha_m|$ are assumed to be equal to 1, thus equation (21) can be re-written as:

$$P_{Rx}^k = |\sqrt{L_{\tau,k}} \sum_{m=1}^M \sum_{n=1}^N |h_{t,km}| |H_{mn}| |h_{rn}| e^{-j(\varphi_{t_{km}} + \eta_m + \varphi_{mn} + \psi_n + \varphi_{rn} + \Omega_k + \Omega_3))}|^2 P_t. \quad (22)$$

2) *Desired User's Rate Maximization Problem:* To this end, substituting (22) in (16) leads to

$$\gamma_k = \frac{|\sqrt{L_{\tau,k}} e^{-j\Omega_3} \mathbf{h}_r^H \mathbf{\Phi}_N \mathbf{H}_{m,n}^H \mathbf{\Phi}_M \mathbf{h}_{t,k}^H e^{-j\Omega_k}|^2 P_t}{\sum_{\substack{i=1 \\ i \neq k}}^K |\sqrt{L_{\tau,i}} e^{-j\Omega_3} \mathbf{h}_r^H \mathbf{\Phi}_N \mathbf{H}_{m,n}^H \mathbf{\Phi}_M \mathbf{h}_{t,i}^H e^{-j\Omega_i}|^2 P_t + \sigma^2}. \quad (23)$$

Therefore to maximize the rate of the desired user under interference, we have

$$\max_{\mathbf{\Phi}_N, \mathbf{\Phi}_M} \log_2(1 + \gamma_k), \quad (24)$$

s.t.

$$\text{C1} : |\phi_m|^2 = 1, \forall m \in \{1, 2, \dots, M\},$$

$$\text{C2} : |\phi_n|^2 = 1, \forall n \in \{1, 2, \dots, N\},$$

(25)

This optimization problem in (24) is NP-hard problem, and the solution is non-trivial, because of the non-convexity due to the constant modulus constraints of IRS 1 and IRS 2 reflecting elements [20], and it is mathematically intractable to obtain an analytical closed form expression of the optimum phases shifts of the two IRSs. The optimal solution will be a balance point between increasing the received SNR of the desired user while decreasing the interference from the other user which are not guaranteed to be aligned sub-objectives. Hence, we find a sub-optimal solution of (24) through maximizing received power of the desired user only.

3) *Sub-optimal Solutions: Maximizing the Received Power of the Desired User:* The total received power of the desired user (e.g. user 1) can be maximized by solving the following system of equations:

$$\eta_m + \psi_n + \varphi_{t_{1m}} + \varphi_{mn} + \varphi_{r_n} + \Omega_1 + \Omega_3 = \nu, \quad \forall m, n. \quad (26)$$

where ν is any constant value, which means that P_{Rx}^k will be maximum when ν is constant $\forall m, n$. In our case, we will choose $\nu = 0$. Thus, equation (26) describes an over-determined system of equations with $M + N$ unknowns, and $M \times N$ equations. We illustrate below equation (26) in more detail:

$$\begin{aligned} \eta_1 + \psi_{M+1} &= -\varphi_{t_k,1} - \varphi_{11} - \varphi_{r,1} - \Omega_{k,1} + \Omega_{3,1}, \\ \eta_m + \psi_{M+n} &= -\varphi_{t_k,m} - \varphi_{mn} - \varphi_{r,n} - \Omega_{k,m} + \Omega_{3,n}, \\ \eta_M + \psi_{M+N} &= -\varphi_{t_k,M} - \varphi_{MN} - \varphi_{r,N} - \Omega_{k,M} + \Omega_{3,N}, \end{aligned} \quad (27)$$

$$\begin{aligned} M \times N \quad & \underbrace{\begin{bmatrix} 1 & 0 & \dots & 0 & 1 & 0 & \dots & 0 \\ 0 & 1 & \ddots & \vdots & 0 & 1 & \ddots & \vdots \\ \vdots & \ddots & \ddots & \vdots & \vdots & \ddots & \ddots & \vdots \\ 0 & \dots & 0 & 1 & 0 & \dots & 0 & 1 \end{bmatrix}}_{M+N} \times \underbrace{\begin{bmatrix} \eta_1 \\ \eta_2 \\ \vdots \\ \eta_m \\ \vdots \\ \eta_{M-1} \\ \eta_M \\ \psi_{M+1} \\ \vdots \\ \psi_{M+n} \\ \vdots \\ \psi_{M+N-1} \\ \psi_{M+N} \end{bmatrix}}_{(M+N) \times 1} = \underbrace{\begin{bmatrix} -\varphi_{t_k,1} - \varphi_{11} - \varphi_{r,1} - \Omega_{k,1} + \Omega_{3,1} \\ \vdots \\ -\varphi_{t_k,M} - \varphi_{M1} - \varphi_{r,1} - \Omega_{k,M} + \Omega_{3,1} \\ \vdots \\ -\varphi_{t_k,1} - \varphi_{12} - \varphi_{r,2} - \Omega_{k,1} + \Omega_{3,2} \\ \vdots \\ -\varphi_{t_k,M} - \varphi_{M2} - \varphi_{r,2} - \Omega_{k,M} + \Omega_{3,1} \\ \vdots \\ -\varphi_{t_k,m} - \varphi_{mn} - \varphi_{r,n} - \Omega_{k,m} + \Omega_{3,n} \\ \vdots \\ -\varphi_{t_k,1} - \varphi_{1N} - \varphi_{r,N} - \Omega_{k,1} + \Omega_{3,N} \\ \vdots \\ -\varphi_{t_k,M} - \varphi_{MN} - \varphi_{r,N} - \Omega_{k,M} + \Omega_{3,N} \end{bmatrix}}_{(M \times N) \times 1} \end{aligned} \quad (28)$$

This is almost always inconsistent and has no solution. However, we solve this problem using sub-optimal mathematical techniques such as pseudo inverse and block solution to obtain the unknowns η_m and ψ_n , calculate Φ_M , Φ_N , and the received power for user 1, and then we compare the results generated from these techniques to those obtained from deep reinforcement

learning solution.

a) *Pseudo-Inverse Solution*: The pseudo-inverse solution for the over-determined system is expressed as follows:

$$\mathbf{A}\mathbf{\Theta} = \mathbf{C}, \quad (29)$$

where $\mathbf{\Theta}$ with dimensions $(M + N) \times 1$ is the matrix that represents IRS₁, and IRS₂ phase shifts from η_1 to ψ_{M+N} , \mathbf{A} with dimensions $(M \times N) \times (M + N)$ represents the binary matrix, and \mathbf{C} with dimensions $(M \times N) \times 1$ represents the matrix containing constant values such as the phase shifts of the transmitter channel $\mathbf{h}_{t,k}^{(t)}$, the phase shifts of the channel between IRS₁ and IRS₂ \mathbf{H}_{mn} , and the phase shifts of the receiver channel $\mathbf{h}_r^{(t)}$.

$$\mathbf{A}^+ = (\mathbf{A}^T \mathbf{A})^{-1} \mathbf{A}^T, \quad (30)$$

where \mathbf{A}^+ is pseudo-inverse of a matrix \mathbf{A} . Thus, the pseudo-inverse solution $\mathbf{\Theta}$ is expressed as

$$\mathbf{\Theta} = \mathbf{A}^+ \mathbf{C}. \quad (31)$$

b) *Block Solution*: Moreover, based on the spatially correlated channel assumption, a low-complexity solution built on the exponential correlation model can be developed and is controlled using the correlation-coefficient ρ between the adjacent RUs. High ρ values lead to high correlation across \mathbf{H}_{mn} elements. This results in two-dimensional blocks of high correlations across the diagonal elements of the channel matrix. Building on this, the SINR can be maximized by selecting one element from each block and replicating its phase response to all other elements in the same block. This solution is denoted as a block solution.

In the case where the channel correlation is very high, the channel \mathbf{H}_{mn} has a block structure, where the elements in the channel matrix form groups, each having the same phase with no correlation between the contiguous blocks. Thus, the number of phases that the IRSs need to compensate for is minimized to the number of blocks in the channel matrix \mathbf{H}_{mn} . Thus, the over-determined system becomes solvable if the number of blocks in the channel matrix $N_{\text{blk}} \leq M + N$, where N_{blk} denotes the number of blocks in the channel.

Therefore, the total received signal power when using the block solution can be rewritten as:

$$P_{Rx}^k = \left| \sqrt{L_{\tau,k}} \sum_{v=1}^V \sum_{w=1}^W |h_{t,kv}| |H_{vw}| |h_{rw}| \right. \\ \left. e^{-j(\varphi_{t_{kv}} + \eta_v + \varphi_{vw} + \psi_w + \varphi_{rw} + \Omega_k + \Omega_3)} \right|^2 P_t, \quad (32)$$

where $V = \frac{M}{N_{\text{blk}}}$, and $W = \frac{N}{N_{\text{blk}}}$ represent the number of blocks, and v, and w represent the index of the blocks in the correlated channel.

Algorithm 1 Block Solution-based Framework

```

1: Input:  $h_t, M, H_{mn}, N, h_t, N_{\text{blk}}$ 
2: Output:  $\eta_n, \psi_m, P_{Rx_k}$ 
3: if  $M + N \leq M \times N$  then
4:   Divide  $\text{IRS}_1$  and  $\text{IRS}_2$  elements into  $N_{\text{blk}}$  blocks.
5:   if  $M + N \geq N_{\text{blk}}$  then
6:     calculate the total received power using (32).
7:   else
8:     if  $M + N < N_{\text{blk}}$  then
9:       Solve (26) using the pseudo-inverse solution, and calculate the total received power using (22).
10:    endif
11:  endif
  
```

Proposition 1. *The total received signal power for each T_{x_k} at the R_x in eq. (22) can be expressed as:*

$$P_{Rx}^k = |\sqrt{L_{\tau,k}} e^{-j\Omega_3} \mathbf{h}_r^H \mathbf{\Phi}_N \mathbf{H}_{mn}^H \mathbf{\Phi}_M \mathbf{h}_{t,k}^H e^{-j\Omega_k}|^2 P_t. \quad (33)$$

The proof is in the Appendix A.

IV. MAXIMIZING THE SUM RATE FOR BOTH USERS

In this section, we provide the mathematical derivations of the optimization problem of our second objective, which is maximizing the sum rate of both users. In particular, in our second objective, we find the optimum phase shifts of IRS 1 and IRS 2 elements that maximize the combined sum rate for all users at the receiver. Moreover, we derive a loose upper bound that is used to benchmark the results of our proposed solutions. The sum rate can be written as

$$R_{\text{sum}} = \sum_{k=1}^K \log_2(1 + \gamma_k). \quad (34)$$

Accordingly, the formulated problem at IRS_1 and IRS_2 is to find out the phase shift matrices $\mathbf{\Phi}_N$, and $\mathbf{\Phi}_M$ that maximizes R_{sum} , and it is expressed as:

$$\max_{\mathbf{\Phi}_N, \mathbf{\Phi}_M} \sum_{k=1}^K \log_2(1 + \gamma_k), \quad (35)$$

s.t.

$$\text{C1} : |\phi_m|^2 = 1, \forall m \in \{1, 2, \dots, M\},$$

$$\text{C2} : |\phi_n|^2 = 1, \forall n \in \{1, 2, \dots, N\},$$

(36)

Similar to the optimization problem in (24) this optimization problem is NP-hard problem, and the solution is non-trivial, because of the non-convexity due to the constant modulus constraints of IRS 1 and IRS 2 reflecting elements [20], and it is

nearly not possible to obtain an analytical solution by mathematical methods for multi-hop IRS optimization. In order to solve it, we leverage DRL technique, specifically DDPG, instead of solving the challenging problem mathematically. The details of the proposed DDPG algorithm are given in section V.

By assuming the case of null interference in (23), a loose upperbound 38 on the sum rates can be determined as follows:
The SINR on user k becomes:

Hence, the upper bound on sum rate can be written as:

V. PROPOSED DDPG FOR CASCADED IRS PHASE CONTROL

In this section, we introduce the scheme of the proposed DDPG algorithm in (see Fig. 2) to solve the optimization problem in (24) and (35) for the cascaded IRS system. Deep Q-Networks are not suitable since they deal with discrete time spaces only. Moreover, the convergence of the policy gradient (PG) algorithm is not sufficient in the context of wireless

communication. DDPG is a model-free reinforcement learning that merges the advantages of both the Q-networks and the PG scheme and overcomes the disadvantages of both algorithms. It utilizes both the continuous state and action spaces [21]. Thus, the optimization problem in (24) and (35) can be solved by learning the policy.

DDPG scheme consists of several key components, which include the agents, state $\mathbf{s}^{(T)}$, the action $\mathbf{a}^{(T)}$, the reward $\mathbf{r}^{(T)}$, the policy function μ , and the Q-value function $Q(\mathbf{s}, \mathbf{a}|\theta^Q)$. The agents operating in our system are the IRS₁ and IRS₂. The states $\mathbf{s}^{(T)}$ in our system are the received SINR for T_{x_1} at the R_x , the received SINR for T_{x_2} at the R_x , and the sum rate for users at time step $(T - 1)$.

The actions $\mathbf{a}^{(T)}$ are the phases of IRS₁ and IRS₂, and the reward $\mathbf{r}^{(T)}$ is the received power for user 1 for our first objective, and the users' sum rate for second objective. Our goal is to optimize the average rewards as this involves instant and future rewards. The DDPG scheme is composed of four neural networks, the critic network, the actor network, the target actor, and the target critic networks to ensure stability.

A. DDPG System Mapping

The initial step in solving the optimization problem of the system model is to map it into the fundamental elements of the DDPG algorithm, specifically, the state space, the action space, and the reward function. Below we discuss the details of this mapping in addition to the general behavior of the DDPG algorithm.

1) *State space*: The state space of the DDPG agent at timestep (T) is represented as follows:

For the first objective:

$$\mathbf{s}^{(T)} = [\gamma_1^{(T-1)}, \gamma_2^{(T-1)}, P_{R_{x_k}}^{(T-1)}], \quad (39)$$

For the second objective:

$$\mathbf{s}^{(T)} = [\gamma_1^{(T-1)}, \gamma_2^{(T-1)}, R_{sum}^{(T-1)}], \quad (40)$$

where $\gamma_1^{(T-1)}$, $\gamma_2^{(T-1)}$, $P_{R_{x_k}}^{(T-1)}$, and $R_{sum}^{(T-1)}$ represent the received SINR for T_{x_1} at the R_x , the received SINR for T_{x_2} at the R_x , the received power for T_{x_1} at the R_x , and the sum rate for users at time step $(T - 1)$ respectively.

2) *Action Space*: The actions are the IRS₁ and IRS₂ phase shift values. The output is an array that defines the phase of each element in the IRS. Thus, the action space is defined by the following policy function:

$$\mathbf{a}^{(T)} = \mu(\mathbf{s}^{(T)}|\theta^\mu) + \mathbf{n}(T) \quad (41)$$

where μ is defined as the policy function and θ^μ represents parameters, weights of neural network, and $\mathbf{n}(T)$ is the Ornstein Uhlenbeck (OU) process-based action noise [22].

Because action space is continuous, the exploration of the action space is handled with the noise that is generated by the OU process. The OU process samples the noise from a correlated normal distribution.

3) *Reward function*: The reward function for the first objective is defined based on the maximum received power for the desired user:

$$r^{(T)} = P_{Rx_k}^{(T)} \quad (42)$$

where $P_{Rx_k}^{(T)}$ is the maximum received power for user 1.

For the second objective, it is defined as the maximum sum rate for users :

$$r^{(T)} = R_{sum}^{(T)} \quad (43)$$

where $R_{sum}^{(T)}$ is the actual sum-rate for the users.

4) *DDPG Algorithm Framework*: The objective of the DDPG algorithm is to train the agents IRS₁ and IRS₂ to take actions that maximize the long-term average reward (i.e. user 1' received power and user's sum rate) throughout the changes of the environments. The agents IRS₁ and IRS₂ adjust the randomized policy and the phases shift matrices in a way that deals with the random environmental statistical behavior to maintain a long-term average reward, rather than an instantaneous response to the channel random changes.

For each iteration, the agents IRS₁ and IRS₂ observe the state which includes the received SINR of the previous state for T_{x1} , $\gamma_1^{(T-1)}$, at the R_x , the received SINR of the previous state for T_{x2} , $\gamma_2^{(T-1)}$, at the R_x , and the reward of the previous state. After that, it calculates the action Φ_M and Φ_N that maximizes the long-term reward. This is accomplished by the actor network, whereas the critic network accepts the state and the action as inputs and outputs the expected reward (i.e. user 1' received power and user's sum rate). After the reward calculation, a new state is observed, and the agents IRS₁ and IRS₂ will modify the phases accordingly till the system learns how to reach the optimal reward. To increase stability, the target actor and critic networks are updated periodically based on the newest actor and critic parameter values.

As revealed in algorithm 2, in step 1 we initialize the replay buffer D of the agent with capacity C . Then we initialize the weights of the actor network and critic network in step 2. In step 3, the actor target network and the critic target network are initialized. The phase shifts for all elements of IRS₁ and IRS₂ are chosen randomly from 0 to 2π at the start of each episode. The following steps from step 4 to step 13 are repeated for each timestep (i.e.iteration). For each timestep, we obtain the following channels $\mathbf{h}_{t,k}^{(T)}$, $\mathbf{h}_{m,n}^{(T)}$, $\mathbf{h}_r^{(T)}$, $\gamma_1^{(T-1)}$, $\gamma_2^{(T-1)}$, and $R_{sum}^{(T-1)}$, observe the state $\mathbf{s}^{(T)}$ for the agents IRS₁ and IRS₂, and the actor network will determine an action $\mathbf{a}^{(T)}$ (i.e. Phase shift matrices) with exploration noise (OU) in step 5. The action $\mathbf{a}^{(T)}$ is reformed into a phase shift matrices for IRS₁ and IRS₂ $\Phi_M = \text{diag}(e^{-j\eta_1}, e^{-j\eta_2}, \dots, e^{-j\eta_M})$ and $\Phi_N = \text{diag}(e^{-j\psi_1}, e^{-j\psi_2}, \dots, e^{-j\psi_N})$. After the agents determine and execute the action, a reward $\mathbf{r}^{(T)}$ is calculated, and a new state $\mathbf{s}^{(T+1)}$ is observed. The state $\mathbf{s}^{(T)}$, action $\mathbf{a}^{(T)}$, reward $\mathbf{r}^{(T)}$, and the new state $\mathbf{s}^{(T+1)}$ are stored as one transition in the replay memory D in steps 6 and 7. Then, the critic network samples a random mini-batch of transitions from the main

memory in step 8 to calculate the target Q-value $\tilde{Q}(\mathbf{s}^{(i)}, \mathbf{a}^{(i)} | \theta^{Q'})$ in step 9 using Bellman equation. In step 10, the weights of the target actor network are updated by minimizing the loss using the obtained target Q-value. In step 11, the weights of the target critic network are updated according to the sampled policy gradient. Finally, the target actor and critic networks are updated using the soft updates τ to increase the learning stability as shown in step 12.

5) *Neural Network Architecture*: The architecture of the DDPG scheme is composed of 4 neural networks which include the actor and critic networks as well as the target actor and target critic networks which are used to improve the stability of the learning process. The target networks are used in the Q-target formula to estimate the value of the future states that are used to train the current networks.

Algorithm 2 DDPG-based Framework

- 1: **Initialization**: Set $T = 0$ and initialize reply buffer of DDPG agent \mathcal{D} with capacity M .
 - 2: Randomly initializes the weights of actor networks θ^μ and critic networks θ^Q .
 - 3: Initialize target networks: $\theta^{\mu'} \leftarrow \theta^\mu$ and $\theta^{Q'} \leftarrow \theta^Q$.
 - 4: **for** $T = 1$ to ∞ **do**
 - 5: Observe state $\mathbf{s}^{(T)}$ and select an action with exploration OU noise $\mathbf{a}^{(T)} = \mu(\mathbf{s}^{(T)} | \theta^\mu) + \mathbf{n}_T$
 - 6: Execute action $\mathbf{a}^{(T)}$ at IRS_1 and IRS_2 .
 - 7: Receive the immediate reward $r^{(T)}$, and observe next state $\mathbf{s}^{(T+1)}$, store transition $(\mathbf{s}^{(T)}, \mathbf{a}^{(T)}, r^{(T)}, \mathbf{s}^{(T+1)})$ in \mathcal{D} .
 - 8: Randomly sample mini-batch transitions from \mathcal{D} :
 $B \leftarrow \{(\mathbf{s}^{(i)}, \mathbf{a}^{(i)}, r^{(i)}, \mathbf{s}^{(i+1)})\} \in \mathcal{D}$.
 - 9: Compute the targets:
 $\tilde{Q}(\mathbf{s}^{(i)}, \mathbf{a}^{(i)} | \theta^{Q'}) = r^{(i)} + \gamma Q(\mathbf{s}^{(i+1)}, \mu(\mathbf{s}^{(i)} | \theta^{\mu'}) | \theta^{Q'})$
 - 10: Update the θ^Q in the critic network by minimizing the loss:
 $L = \frac{1}{|B|} \sum_{i=1}^{|B|} (\tilde{Q}(\mathbf{s}^{(i)}, \mathbf{a}^{(i)} | \theta^{Q'}) - Q(\mathbf{s}^{(i)}, \mathbf{a}^{(i)} | \theta^Q))^2$
 - 11: Update the θ^μ in actor network according to the sampled policy gradient:
 $\nabla_{\theta^\mu} J \approx \frac{1}{|B|} \sum_{i=1}^{|B|} \nabla_a Q(\mathbf{s}^{(i)}, \mathbf{a}^{(i)} | \theta^Q) \nabla_{\theta^\mu} \mu(\mathbf{s}^{(i)} | \theta^\mu)$
 - 12: Update the target networks:
 $\theta^{Q'} \leftarrow \tau \theta^Q + (1 - \tau) \theta^{Q'}$
 $\theta^{\mu'} \leftarrow \tau \theta^\mu + (1 - \tau) \theta^{\mu'}$
 - 13: **end for**
-

B. Complexity Analysis

To reveal the complexity of the DRL algorithm, we demonstrate a quantitative analysis of the proposed DRL-based algorithm \mathcal{C}_{DRL} versus the complexity of pseudo-inverse, block solution, and exhaustive search methods. The DRL algorithm is a neural network-based algorithm and its architecture possesses the multi-layer perceptron (MLP) structure, which is a fully connected class of feed-forward artificial neural network (ANN). Thus, the complexity of the forward pass in MLP is a vector or matrix multiplication. For our system, the evaluation of the DRL complexity depends mainly on the calculations throughout the exploitation phase. Hence, we are interested in the complexity of the trained network (steady-state) which relies heavily on the actor network (i.e. forward network architecture).

Deep neural networks are composed of multiple layers, an input layer, an output layer, and hidden layers. We assume that S is the number of states, which is the size of the actor network's input, U_i is the number of neurons in each layer's input, n is the number of hidden layers, U_j is the number of neurons in each layer's output, A is the number of actions, which is the size of the actor network's output. Thus, the complexity of the input layer is $O(S \times U_i)$, the complexity of the hidden layers is $O(n \times U_i \times U_j)$, and the complexity of the output layer is $O(U_j \times A)$. Hence, the overall complexity of the DRL

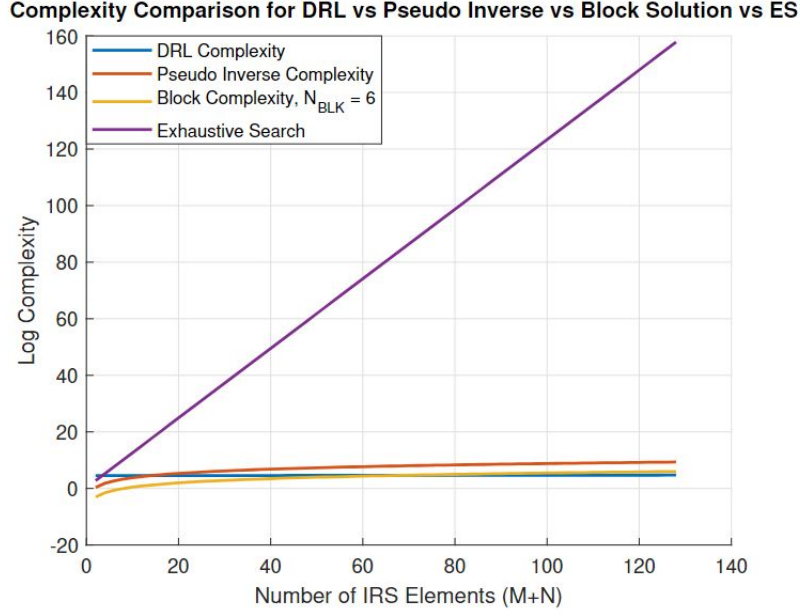


Figure 3: Complexity of DRL vs. Pseudo Inverse vs. Block Solution. $M=N=64$, $N_{BLK} = 6$.

algorithm is

$$\mathcal{C}_{DRL} = S \times Ui + n \times Ui \times Uj + Uj \times A. \quad (44)$$

Further, the DRL algorithm will always select the action A that yields the highest reward, and performs a linear search on the output. Therefore, the overall computational complexity of one forward pass in the neural network is expressed as [23]:

$$\mathcal{C}_{DRL} = S \times Ui + n \times Ui \times Uj + Uj \times A + A. \quad (45)$$

On the other hand, the pseudo-inverse solution of a matrix \mathcal{A} with size $MN \times (M+N)$ can be calculated from its singular value decomposition (SVD) as $O((MN)^2 \times (M+N))$, where $MN > (M+N)$, and M and N are the number of elements in IRS_1 and IRS_2 respectively [24], [25]. However, for the block solution, the complexity of a matrix \mathcal{A} with size $\frac{MN}{N_{blk}^2} \times \frac{M+N}{N_{blk}}$ is reduced to $O((\frac{MN}{N_{blk}^2})^2 \times (\frac{M+N}{N_{blk}}))$, where $N_{blk} < (M+N)$.

Moreover, the complexity of the exhaustive scheme \mathcal{C}_{ES} assuming K users, M elements for IRS_1 , and N elements for IRS_2 , and phase search steps $\Xi = \lfloor \frac{2\pi}{\Delta\Phi} \rfloor$, can be expressed as

$$\mathcal{C}_{ES} = O(K \times (\Xi + 1)^{(M+N)}). \quad (46)$$

Thus, the complexity of the DRL algorithm is much lower than that of the pseudo-inverse, block solution, and exhaustive search methods as the number of IRS elements increases as shown in the following figures Fig. 3, and Fig. 4.

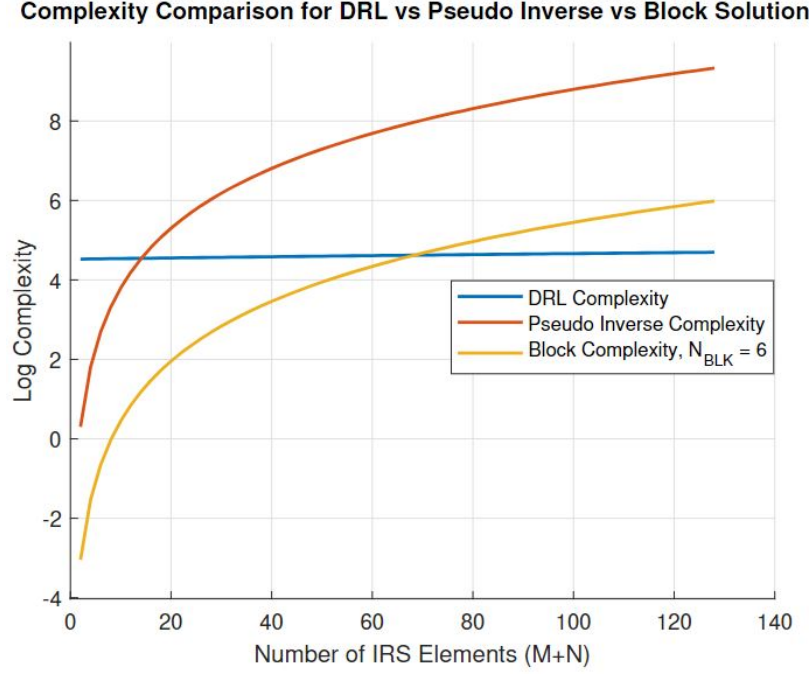


Figure 4: Complexity of DRL vs. Pseudo Inverse vs. Block Solution vs. Exhaustive Search. $M=N=64$, $N_{BLK} = 6$.

VI. SIMULATION RESULTS

In this section, we evaluate the performance of the proposed DDPG-based cascaded IRS-assisted wireless THz communications. To reveal the performance of our DDGP system, we need to compare it with a benchmark scheme considering the scenario of maximizing the rate for the desired user, and the scenario of maximizing the sum rate for both users. Therefore, when maximizing the rate for the desired user (i.e. user 1), we provide two benchmarking schemes as reference models for our system with reflecting elements $M = 18$ for IRS₁, and $N = 18$ for IRS₂; the first scheme is based on pseudo-inverse, and the second is based on block solution. Further, when maximizing the sum rate for both users, we compare the sum rates obtained from using the DDPG algorithm to a discretized exhaustive search approximation to prove that our DDPG scheme performance is close to the exhaustive search. We employ this procedure to find out the optimum phase shift matrices that result in an approximation to the maximum sum rate. To avoid the high complexity of the exhaustive search algorithm, we consider a limited number of reflecting elements $M = 4$ for IRS₁, and $N = 4$ for IRS₂. For each IRS₁ and IRS₂ element, we consider the phase shifts between 0 and 2π with a search step of $2\pi/72$. This will give us $(72+1)^{M+N}$ combinations of phase shift reflection matrices. After obtaining the optimum phase shift matrices, we calculate the sum rates accordingly for users. Moreover, we compare the DDPG sum rates to those calculated based on random phase generation (i.e. without optimization) as another way to benchmark our system.

The default parameters used in the simulation for the DDPG-based cascaded IRS algorithm are shown in Table 2. The number of reflecting elements used for IRS₁ and IRS₂ is 18. The number of users is $K = 2$, the number of antennas per user is $N_t = 1$ the number of antennas at the receiver is $N_r = 1$, and the wavelength is $\lambda = 10^{-3}$. The channel between user 1 and IRS₁, user 2 and IRS₁, IRS₂, and the receiver follows the rician fading model with rician factor $K_1 = K_2 = 10$. The path loss exponent for the channel between the transmitters and IRS₁ is 2, and the path loss exponent for the channel

between IRS₂ and the receiver is 2. The carrier frequency is $f = 300 \times 10^9$, the bandwidth is $BW = 2 \times 10^9$, the noise spectral density $N_{PSD} = -174$ dB/Hz, and the noise figure at the receiver $F_{dB} = 10$ dB. Moreover, the coordinates for IRS₁ is $(x_{r1} = 5, y_{r1} = 10, h_{r1} = 12)$, the coordinates for IRS₂ is $(x_{r2} = 10, y_{r2} = 10, h_{r2} = 12)$, the distance between user 1 and IRS₁ is variable with range between $r_{t1} = 3$ m and 15 m, the distance between user 2 and IRS₁ is 15 m, and the reflection coefficients of IRS₁ and IRS₂ is $\alpha = 1$. The coordinates of the receiver R_x is $(x_{rx} = 20, y_{rx} = 0, h_r = 5)$. The antenna diameter is $D_t = 0.12$ m. The height of user 1 and user 2 is $h_t = 5$. We define the distance ratio as the distance r_{t1} between user 1 and IRS₁, divided by the distance r_{t2} between user 2 and IRS₁. Numerical results for the sum rates are calculated using 10^3 Monte-Carlo simulations.

The proposed DDPG scheme is composed of actor and critic networks. Both networks are dense neural networks (DNN) with 4 layers. Each layer is nn.Linear and accepts two parameters, the first is the input size and the second is the output size. For the actor network, the states are the input with a size equal to 3 neurons, and the output is the action with size of 36 neurons. In addition to the input and output layers, there are two hidden layers each that accepts 128 neurons as input and outputs 128 neurons, followed by the ReLU activation function. To provide enough gradient, the output layer of the actor network uses the tanh(\cdot). For the critic network, the input consists of the number of states and the number of actions, both are concatenated to represent the input of the critic network. This is followed by two hidden layers between the input layer and the output layer, each that accepts 128 neurons as input, and outputs 128 neurons, followed by the ReLU activation function. The output layer of the critic network represents the Q-value with 36 neurons. To update the parameters, both actor and critic networks use Adam optimizer. Furthermore, the results are generated by considering the average rate for over 1000 iterations. The learning rate of the actor network is set to 3×10^{-4} , and the learning rate of the critic network is set to 1×10^{-4} . The discount factor of the future reward Γ , the batch size is equal to 128, the replay buffer \mathcal{C} is equal to 10^5 , and the number of episodes is 10000.

The generated results shown in Fig. 5 reveal the convergence of the DDPG algorithm. The figure shows the rewards versus the episodes, and that the rewards are increasing with time. This reveals that the learning process is conducted successfully.

A. Simulation Results for Maximizing The Received Power At The Receiver R_x

In the following simulations, we demonstrate the results for maximizing the rate for the desired user (i.e. user 1) at the receiver by plotting the rate of user 1 versus the distance ratio between user 1 and user 2 utilizing various schemes such as DDPG, block solution, and pseudo-inverse solution methods.

Fig. 6 and Fig. 7 shows user 1's rate for the DDPG scheme versus the distance ratio between 0.2 and 1. As the distance ratio increases, the data rate for user 1 decreases, because user 2 will be closer to user 1, and thus the interference from user 2 to user 1 increases. Moreover, Fig. 6a shows that user 1's rate for the DDPG scheme exceeds that of pseudo-inverse and block-solution methods with a correlation-coefficient ρ equal to 1.0. This reveals the effectiveness of the DDPG algorithm and that it is superior to pseudo-inverse and block-solution.

Furthermore, the following figures Fig. 6b Fig. 6c, Fig. 7a, and Fig. 7b demonstrate that when the correlation-coefficient ρ decreases, user's 1 rate decreases for DDPG algorithm, block-solution, and pseudo-inverse solution. This shows the importance

Table 2: Parameters Used in Simulation

Simulation Parameters	Values
Number of Users (K)	2
Number of antennas per user N_t	1
Number of antennas at the receiver N_r	1
Speed of the light c	3×10^8
Carrier Frequency f	300×10^9
Wavelength λ	1×10^{-3}
Number of IRS ₁ Reflecting Elements (M)	18
Number of IRS ₂ Reflecting Elements (N)	18
X-axis of IRS ₁ x_{r1}	5
Y-axis of IRS ₁ y_{r1}	10
X-axis of IRS ₂ x_{r2}	10
Y-axis of IRS ₂ y_{r2}	10
height of IRS ₁ h_{r1}	12
height of IRS ₂ h_{r2}	12
Distance between User 1 and IRS ₁	3 to 15
Distance between User 2 and IRS ₁	15
Heights of User 1 and User 2 h_t	5
IRS ₁ and IRS ₂ Reflection Coefficients α	1
IRS ₁ and IRS ₂ half-power Spacing d_x	$\lambda/2$
IRS ₁ and IRS ₂ Element Spacing d_y	$\lambda/2$
Antenna diameter in meters D_t	0.12
X-axis of Rx x_{rx}	20
Y-axis of Rx y_{rx}	0
height of Rx h_r	5
Bandwidth	2×10^9 MHz
Noise power spectral density N_{PSD}	-174 dB/Hz
Noise figure at the receiver F_{dB}	10
Average Noise power in dB N_0	-174 dB/Hz
Noise power in linear scale no	7.9621×10^{-11}
Transmitters to IRS ₁ Path loss exponent	2
IRS ₂ to receiver R_x Path loss exponent	2
Rician Factor	10
Critic Network learning rate	3×10^{-4}
Actor Network learning rate	1×10^{-4}
Target Critic Network learning rate	3×10^{-4}
Target Actor Network learning rate	1×10^{-4}
Discount factor of the future reward Γ	0.99
Coefficient of Soft Updates τ	1×10^{-3}
Batch size	128
Replay Buffer Capacity \mathcal{C}	10^5
Number of episodes	10000

of correlation channels in our scenario and their benefit in increasing the data rate. On top of that, the DDPG scheme still achieves higher rates than block-solution and the pseudo-inverse solution even when the correlation-coefficient ρ decreases. On the other hand, it is important to note that, for low values of correlation-coefficient ρ the difference between the DDPG's data rates and other schemes retracts.

Fig. 8 demonstrate the rates for the DDPG scheme versus the distance-ratio for various correlation-coefficients. It is clear that when the correlation-coefficient ρ increases the data rates for the DDPG scheme increase, since increasing the value of correlation, will increase the learning efficiency of the DDPG algorithm. Thus, the DDPG scheme achieves higher data rates

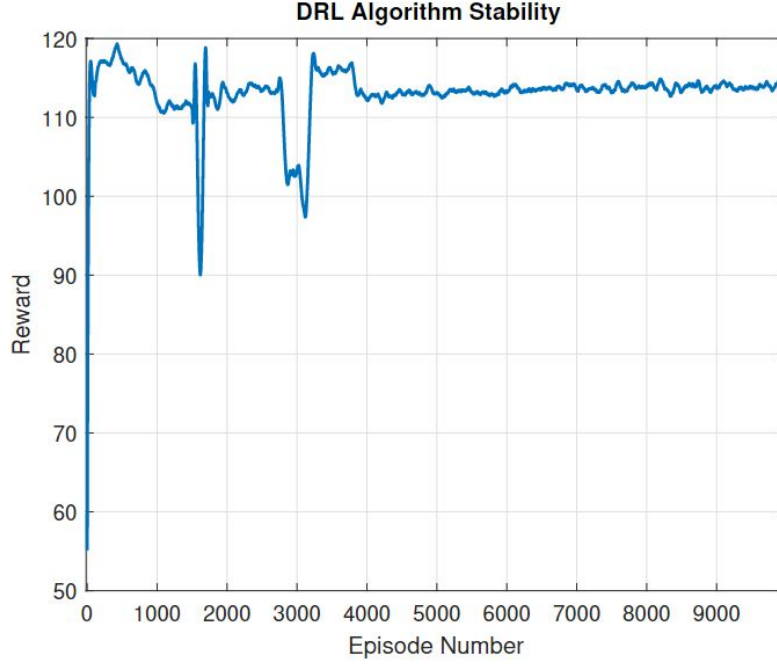


Figure 5: DDPG algorithm convergence. Rewards vs Episodes.

than other methods especially when the correlation-coefficient ρ is high.

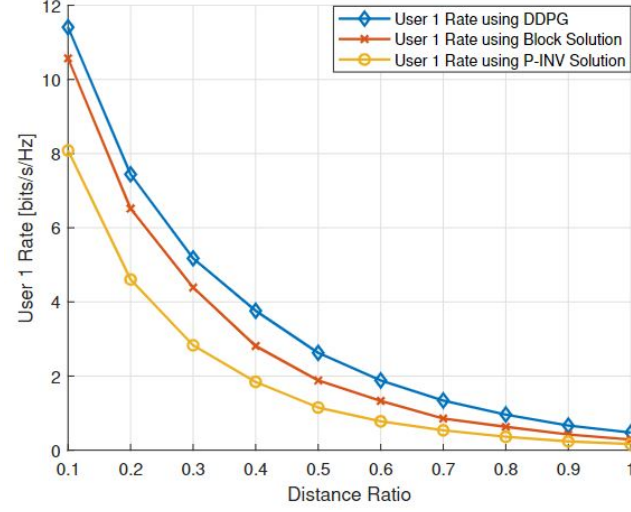
B. Simulation Results for Maximizing the Sum Rate for Both Users

In the following simulations, we show the results for maximizing the sum rate for both users at the receiver. We plot the sum rate versus the distance ratio between user 1 and user 2 utilizing the DDPG method for various correlation coefficients as shown in Fig. 9. It is obvious from the results that the sum rates obtained from the DDPG solution increase with the increase of the correlation-coefficient ρ .

Further, in all our simulations, constant learning rates were used for our proposed DDPG scheme, which is 10^{-4} for actor network, and 3×10^{-4} for the critic network. The influence of the learning rate on the DDPG data rates is shown in Fig. 10, which reveals a comparison between different learning rates, i.e., 10^{-3} , 10^{-4} , 10^{-5} for actor network, and 3×10^{-3} , 3×10^{-4} , 3×10^{-5} for critic network. Thus, the highest DDPG rate is achieved when the actor networks' learning rate equals 10^{-4} and the critic networks' learning rate equals 3×10^{-4} . Therefore, the average rewards are determined by the learning rates (e.g. 10^{-4}). Too small learning rates 10^{-5} or too large learning rates 10^{-3} produce lower average rewards, where the learning rate 10^{-4} achieves better rewards.

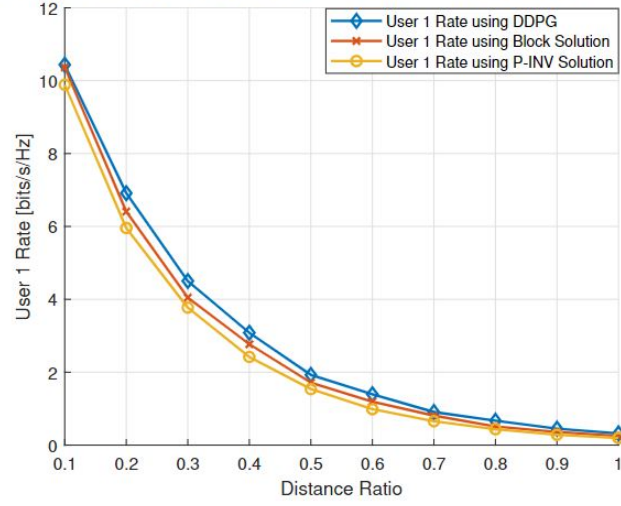
To verify the performance of our DDPG scheme, we compare the sum rates produced by the DDPG algorithm to the discretized exhaustive search algorithm that is used to calculate the maximum sum rate by obtaining the optimum phase shift matrix. The complexity of the exhaustive search is too much high so the number of reflecting elements used for IRS₁ is $M = 4$, and for IRS₂ is $N = 4$ rather than $M = N = 18$. For each IRS element, we take into consideration the phases between 0 and 2π with a search step size equal to $\frac{2\pi}{72}$. Thus the number of combinations for the phase shift matrices is equal to $(72 + 1)^4$. The sum rates are calculated for two users and 100 Monte-Carlo simulations. The results are revealed in Fig. 11 where the

User 1 Rate, Correlation Coefficient $\rho = 1$, $M=N=18$, User1 is closer to IRS1



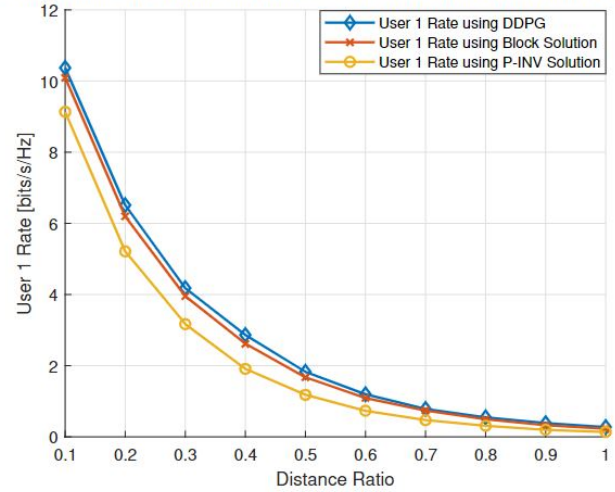
(a) Correlation-Factor ρ equal to 1.0.

User 1 Rate, Correlation Coefficient $\rho = 0.9$, $M=N=18$, User1 is closer to IRS1



(b) Correlation-Factor ρ equal to 0.9.

User 1 Rate, Correlation Coefficient $\rho = 0.75$, $M=N=18$, User1 is closer to IRS1



(c) Correlation-Factor ρ equal to 0.75.

Figure 6: User 1's Rate vs Distance ratio

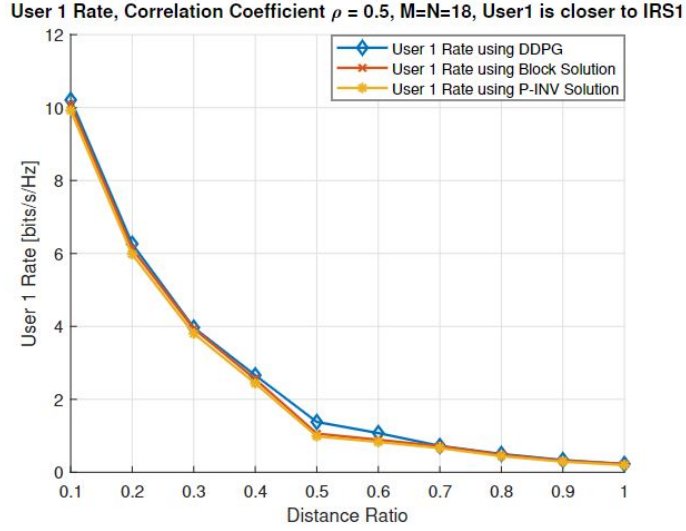
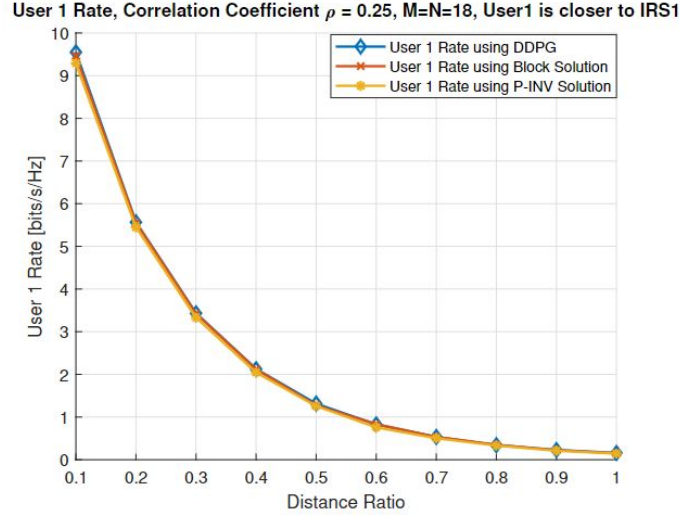
(a) Correlation-Factor ρ equal to 0.5.(b) Correlation-Factor ρ equal to 0.25.

Figure 7: User 1's Rate vs Distance ratio

DDPG algorithm sum rates are close to the exhaustive search with the specified granularity.

VII. CONCLUSION

In this paper, we considered the uplink multiple access scenario of the cascaded IRS system to combat the short-range communications in THz networks, intending to achieve two objectives. The first objective is to maximize the rate of the desired user. We showed that the problem is non-convex and finding a closed form expression is mathematically intractable. Therefore, we proposed two sub-optimal solution for maximizing the received power of the desired user. The second objective is to maximize the sum rate for both users which is also non-convex problem and more complicated. We employed the DDPG algorithms which are capable of coping with non-convex optimization problems to solve the maximization problem for the cascaded IRS system. DDPG algorithm obtains the optimum IRS phases that maximize the received rate for the desired user, and the sum rate for both users. Simulation results for the first objective reveal that DDPG can achieve higher data rates than sub-optimal methods, pseudo-inverse and block-solution. For the second objective, it is clear that the DDPG sum rates are

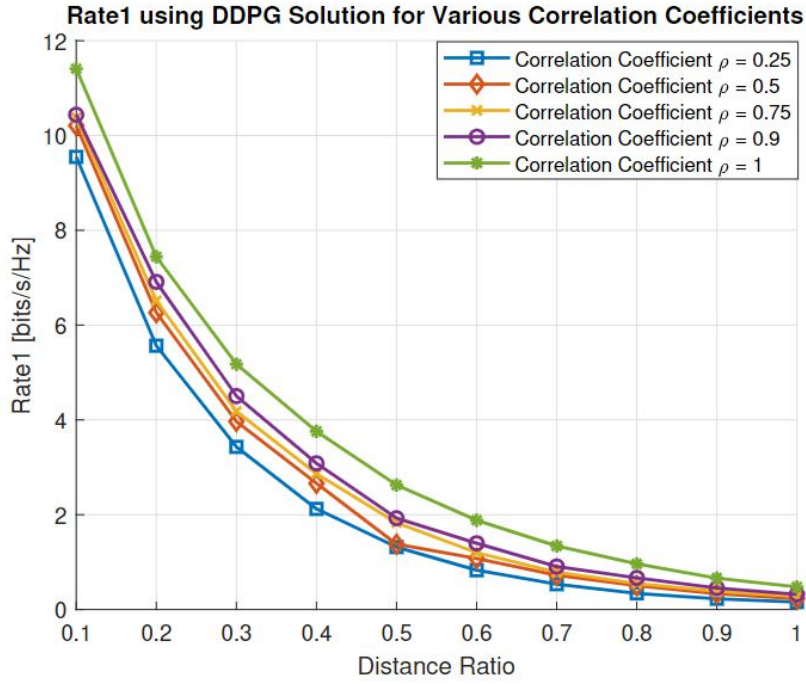


Figure 8: User 1's Rate for DDPG vs Distance ratio for Various correlation-coefficients ρ . $M=N=18$.

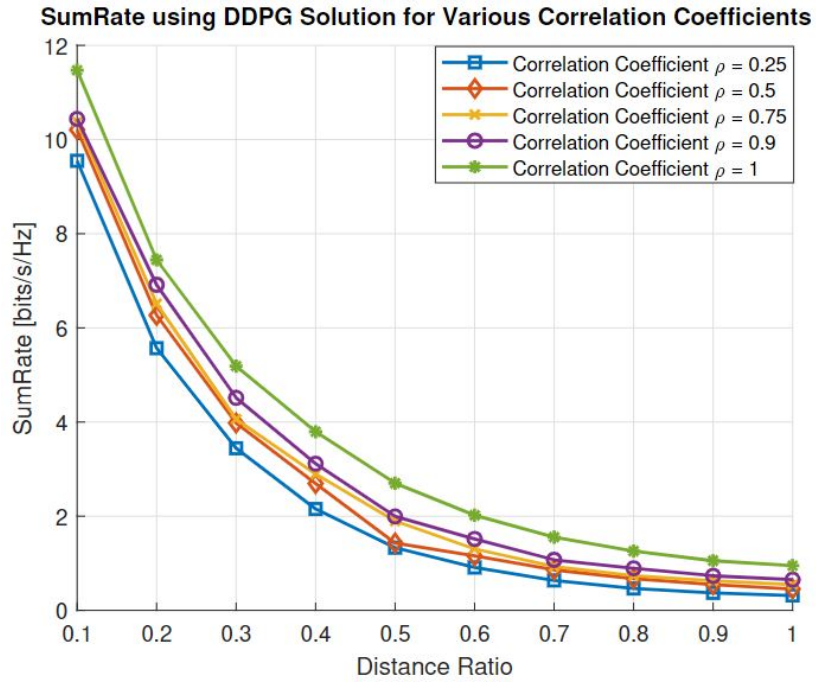


Figure 9: DDPG Sum Rate vs Distance ratio for Various correlation-coefficients ρ . $M=N=18$.

DDPG SumRate for Various Learning Rates and Correlation Coefficient $\rho=1$

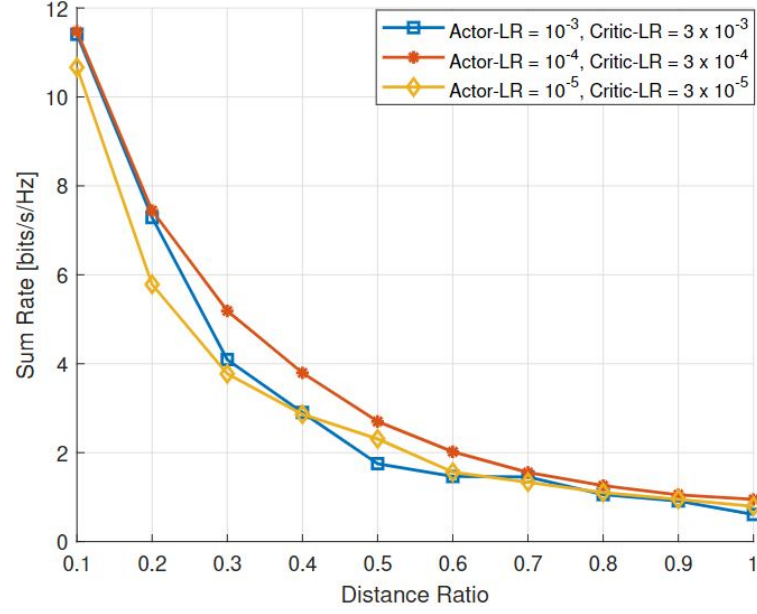


Figure 10: DDPG Sum Rate vs Distance ratio for Various learning rates and correlation-coefficient $\rho = 1.0$. $M=N=18$.

DDPG SumRate vs Upperbound vs ES for $\rho=0.9$ and $M=N=4$

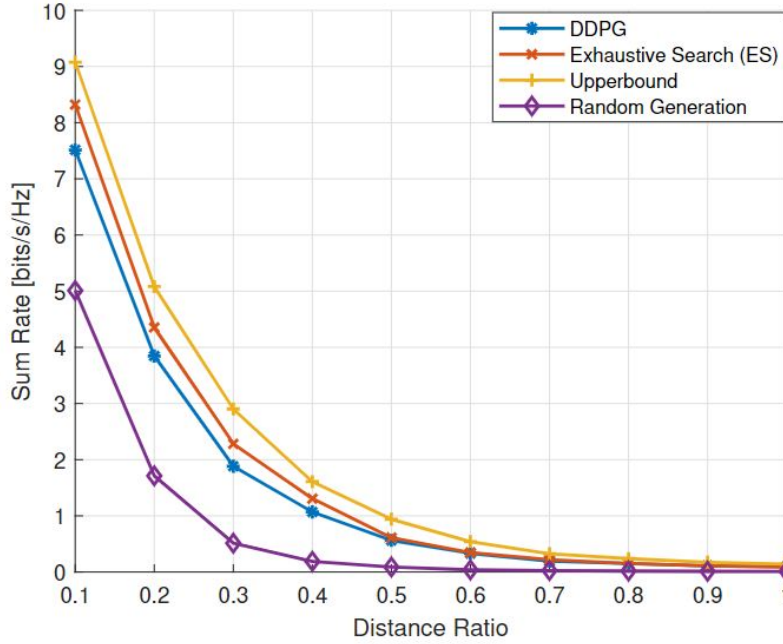


Figure 11: Comparison between DDPG Sum Rate, exhaustive search, and upper bound vs Distance Ratio for Various correlation-coefficients $\rho = 0.9$. $M=N=4$.

close to the discretized exhaustive search with a search step equal to $2 * \pi / 72$. Further, DDPG reveals the significance of the correlation in the channels to enhance the learning process and achieve higher data rates.

REFERENCES

- [1] C. Chaccour, M. N. Soorki, W. Saad, M. Bennis, P. Popovski and M. Debbah, "Seven Defining Features of Terahertz (THz) Wireless Systems: A Fellowship of Communication and Sensing," in IEEE Communications Surveys and Tutorials, DOI: 10.1109/COMST.2022.3143454.
- [2] R. Imran, M. Odeh, N. Zorba and C. Verikoukis, "Quality of Experience for Spatial Cognitive Systems within Multiple Antenna Scenarios," in IEEE Transactions on Wireless Communications, vol. 12, no. 8, pp. 4153-4161, August 2013, doi: 10.1109/TWC.2013.071113.122037.
- [3] I. Yildirim, A. Uyrus and E. Basar, "Modeling and Analysis of Reconfigurable Intelligent Surfaces for Indoor and Outdoor Applications in Future Wireless Networks," in IEEE Transactions on Communications, vol. 69, no. 2, pp. 1290-1301, Feb. 2021, doi: 10.1109/TCOMM.2020.3035391.
- [4] Z. Chen, X. Ma, C. Han and Q. Wen, "Towards intelligent reflecting surface empowered 6G terahertz communications: A survey," in China Communications, vol. 18, no. 5, pp. 93-119, May 2021, DOI: 10.23919/JCC.2021.05.007.
- [5] T. V. Nguyen, T. P. Truong, T. M. T. Nguyen, W. Noh, and S. Cho, "Achievable Rate Analysis of Two-Hop Interference Channel with Coordinated IRS Relay," in IEEE Transactions on Wireless Communications, DOI: 10.1109/TWC.2022.3154372.
- [6] W. Mei and R. Zhang, "Multi-Beam Multi-Hop Routing for Intelligent Reflecting Surfaces Aided Massive MIMO," in IEEE Transactions on Wireless Communications, vol. 21, no. 3, pp. 1897-1912, March 2022, DOI: 10.1109/TWC.2021.3108020.
- [7] Q. Sun, P. Qian, W. Duan, J. Zhang, J. Wang and K. -K. Wong, "Ergodic Rate Analysis and IRS Configuration for Multi-IRS Dual-Hop DF Relaying Systems," in IEEE Communications Letters, vol. 25, no. 10, pp. 3224-3228, Oct. 2021, DOI: 10.1109/LCOMM.2021.3100347.
- [8] Z. Zhang and Z. Zhao, "Weighted Sum-Rate Maximization for Multi-Hop RIS-Aided Multi-User Communications: A Minorization-Maximization Approach," 2021 IEEE 22nd International Workshop on Signal Processing Advances in Wireless Communications (SPAWC), 2021, pp. 106-110, DOI: 10.1109/SPAWC51858.2021.9593114.
- [9] A. Almohamad, M. Hasna, N. Zorba, and T. Khattab, "Performance of THz Communications Over Cascaded RISs: A Practical Solution to the Over-Determined Formulation," in IEEE Communications Letters, vol. 26, no. 2, pp. 291-295, Feb. 2022, DOI: 10.1109/LCOMM.2021.3132655.
- [10] C. Huang et al., "Hybrid Beamforming for RIS-Empowered Multi-hop Terahertz Communications: A DRL-based Method," 2020 IEEE Globecom Workshops (GC Wkshps, Taipei, Taiwan, 2020, pp. 1-6, doi: 10.1109/GCWkshps50303.2020.9367503.
- [11] C. Huang et al., "Multi-Hop RIS-Empowered Terahertz Communications: A DRL-Based Hybrid Beamforming Design," in IEEE Journal on Selected Areas in Communications, vol. 39, no. 6, pp. 1663-1677, June 2021, DOI: 10.1109/JSAC.2021.3071836.
- [12] C. Soni and N. Gupta, "Channel Estimation of Spatial Correlated Channel in Massive MIMO," 2021 8th International Conference on Computing for Sustainable Global Development (INDIACom), New Delhi, India, 2021, pp. 836-841.
- [13] K. Feng, Q. Wang, X. Li and C. -K. Wen, "Deep Reinforcement Learning Based Intelligent Reflecting Surface Optimization for MISO Communication Systems," in IEEE Wireless Communications Letters, vol. 9, no. 5, pp. 745-749, May 2020, doi: 10.1109/LWC.2020.2969167.
- [14] N. Zorba and A. I. Perez-Neira, "Opportunistic Grassmannian Beamforming for Multiuser and Multiantenna Downlink Communications," in IEEE Transactions on Wireless Communications, vol. 7, no. 4, pp. 1174-1178, April 2008, doi: 10.1109/TWC.2008.060972.
- [15] B. Zheng, C. You and R. Zhang, "Efficient Channel Estimation for Double-IRS Aided Multi-User MIMO System," in IEEE Transactions on Communications, vol. 69, no. 6, pp. 3818-3832, June 2021, doi: 10.1109/TCOMM.2021.3064947.
- [16] B. Zheng, C. You, W. Mei, and R. Zhang, "A Survey on Channel Estimation and Practical Passive Beamforming Design for Intelligent Reflecting Surface Aided Wireless Communications," in IEEE Communications Surveys and Tutorials, vol. 24, no. 2, pp. 1035-1071, Second quarter 2022, doi: 10.1109/COMST.2022.3155305.
- [17] X. Hu, R. Zhang and C. Zhong, "Semi-Passive Elements Assisted Channel Estimation for Intelligent Reflecting Surface-Aided Communications," in IEEE Transactions on Wireless Communications, vol. 21, no. 2, pp. 1132-1142, Feb. 2022, doi: 10.1109/TWC.2021.3102446.
- [18] K. Ntontin et al., "Reconfigurable Intelligent Surface Optimal Placement in Millimeter-Wave Communications," 2021 15th European Conference on Antennas and Propagation (EuCAP), Dusseldorf, Germany, 2021, pp. 1-5, doi: 10.23919/EuCAP51087.2021.9411076.
- [19] J. Kokkonen, J. Lehtomäki and M. Juntti, "Simplified molecular absorption loss model for 275–400 gigahertz frequency band," 12th European Conference on Antennas and Propagation (EuCAP 2018), 2018, pp. 1-5, DOI: 10.1049/cp.2018.0446.
- [20] M. Shehab, B. S. Ciftler, T. Khattab, M. M. Abdallah and D. Trinchero, "Deep Reinforcement Learning Powered IRS-Assisted Downlink NOMA," in IEEE Open Journal of the Communications Society, vol. 3, pp. 729-739, 2022, doi: 10.1109/OJCOMS.2022.3165590.

- [21] V. François-Lavet, P. Henderson, R. Islam, M. Bellemare, and J. Pineau (2018), "An Introduction to Deep Reinforcement Learning", Foundations and Trends in Machine Learning: Vol. 11, No. 3-4, 2018.
- [22] G E. Uhlenbeck and L S. Ornstein, "On the Theory of the Brownian Motion", Revista Latinoamericana De Microbiologia, 1930.
- [23] M. Elsayed, A. Badawy, A. E. Shafie, A. Mohamed and T. Khattab, "A Deep Reinforcement Learning Framework for Data Compression in Uplink NOMA-SWIPT Systems," in IEEE Internet of Things Journal, vol. 9, no. 14, pp. 11656-11674, 15 July15, 2022, doi: 10.1109/IJOT.2021.3131524.
- [24] Keller-Gehrig, Walter: Fast algorithms for the characteristic polynomial. Theoretical Computer Science, 36(2-3):309–317, 1985, ISSN 0304-3975. [http://dx.doi.org/10.1016/0304-3975\(85\)90049-0](http://dx.doi.org/10.1016/0304-3975(85)90049-0). [x.doi.org/10.1145/345542.345644](https://doi.org/10.1145/345542.345644).
- [25] V. Vasudevan, M. Ramakrishna, "A Hierarchical Singular Value Decomposition Algorithm for Low Rank Matrices,". 2017-10-08 | Preprint. ARXIV: arXiv:1710.02812v2.

APPENDIX

A. Proof of Proposition 1 (See page 12)

The total received signal power for each T_{x_k} at the R_x in eq. (22) can be expressed as:

$$P_{Rx}^k = |\sqrt{L_{\tau,k}} e^{-j\Omega_3} \mathbf{h}_r^H \Phi_N \mathbf{H}_{m,n}^H \Phi_M \mathbf{h}_{t,k}^H e^{-j\Omega_k}|^2 P_t.$$

Proof. • Multiply the receiver channel \mathbf{h}_r^H by IRS₂ phase shift reflection matrix Φ_N :

$$\begin{aligned} \left[\mathbf{h}_r^H \Phi_N \right] &= \underbrace{\left[h_{r1}^*, \dots, h_{rn}^*, \dots, h_{rN}^* \right]}_{1 \times N} \times \underbrace{\begin{bmatrix} e^{-j\psi_1} & 0 & \dots & \dots & \dots & 0 \\ 0 & e^{-j\psi_2} & 0 & \ddots & \ddots & 0 \\ \vdots & 0 & \ddots & \ddots & \ddots & \vdots \\ \vdots & \ddots & \ddots & e^{-j\psi_n} & \ddots & \vdots \\ \vdots & \ddots & \ddots & \ddots & \ddots & \vdots \\ 0 & \dots & \dots & \dots & 0 & e^{-j\psi_N} \end{bmatrix}}_{N \times N} \\ \left[\mathbf{h}_r^H \Phi_N \right] &= \underbrace{\left[h_{r1}^* e^{-j\psi_1}, \dots, h_{rn}^* e^{-j\psi_n}, \dots, h_{rN}^* e^{-j\psi_N} \right]}_{1 \times N} \end{aligned}$$

• Multiply the result of the previous operation by $\mathbf{h}_{m,n}^H$:

$$\begin{aligned} \left[\mathbf{h}_r^H \Phi_N \mathbf{H}_{mn}^H \right] &= \underbrace{\left[h_{r1}^* e^{-j\psi_1}, \dots, h_{rn}^* e^{-j\psi_n}, \dots, h_{rN}^* e^{-j\psi_N} \right]}_{1 \times N} \times \underbrace{\begin{bmatrix} h_{11}^* & h_{21}^* & \dots & \dots & \dots & h_{M1}^* \\ h_{12}^* & h_{22}^* & \ddots & \ddots & \ddots & h_{M2}^* \\ \vdots & \ddots & \ddots & \ddots & \ddots & \vdots \\ \vdots & \ddots & \ddots & H_{mn}^* & \ddots & \vdots \\ \vdots & \ddots & \ddots & \ddots & \ddots & \vdots \\ h_{1N}^* & \dots & \dots & \dots & \dots & h_{MN}^* \end{bmatrix}}_{N \times M} \\ \left[\mathbf{h}_r^H \Phi_N \mathbf{H}_{mn}^H \right] &= \underbrace{\left[\sum_{n=1}^N h_{rn}^* e^{-j\psi_n} h_{1n}^*, \sum_{n=1}^N h_{rn}^* e^{-j\psi_n} h_{2n}^*, \dots, \sum_{n=1}^N h_{rn}^* e^{-j\psi_n} h_{MN}^* \right]}_{1 \times M} \end{aligned}$$

• Multiply the result of the previous operation by IRS₁ phase shift reflection matrix Φ_M :

$$\left[\mathbf{h}_r^H \Phi_N \mathbf{H}_{mn}^H \Phi_M \right] =$$

$$\begin{aligned}
& \underbrace{\left[\sum_{n=1}^N h_{rn}^* e^{-j\psi_n} h_{1n}^*, \sum_{n=1}^N h_{rn}^* e^{-j\psi_n} h_{2n}^*, \dots, \sum_{n=1}^N h_{rn}^* e^{-j\psi_n} H_{MN}^* \right]}_{1 \times M} \times \underbrace{\begin{bmatrix} e^{-j\eta_1} & 0 & \dots & \dots & \dots & 0 \\ 0 & e^{-j\eta_2} & 0 & \ddots & \ddots & 0 \\ \vdots & 0 & \ddots & \ddots & \ddots & \vdots \\ \vdots & \ddots & \ddots & e^{-j\eta_m} & \ddots & \vdots \\ \vdots & \ddots & \ddots & \ddots & \ddots & \vdots \\ 0 & \dots & \dots & \dots & 0 & e^{-j\eta_M} \end{bmatrix}}_{M \times M} \\
& \left[\mathbf{h}_r^H \Phi_N \mathbf{H}_{mn}^H \Phi_M \right] = \underbrace{\left[\sum_{m=1}^M \sum_{n=1}^N h_{rn}^* e^{-j\psi_n} H_{mn}^* e^{-j\eta_m} \right]}_{1 \times M}
\end{aligned}$$

- Multiply the result of the previous operation by the transmitter channel of user K $\mathbf{h}_{t,k}^H$:

$$\left[\mathbf{h}_r^H \Phi_N \mathbf{H}_{mn}^H \Phi_M \mathbf{h}_{t,k}^H \right] = \underbrace{\left[\sum_{m=1}^M \sum_{n=1}^N h_{rn}^* e^{-j\psi_n} H_{mn}^* e^{-j\eta_m} \right]}_{1 \times M} \times \underbrace{\begin{bmatrix} h_{t,k,1}^* \\ h_{t,k,2}^* \\ \vdots \\ h_{t,k,M}^* \end{bmatrix}}_{M \times 1}$$

$$\mathbf{h}_r^H \Phi_N \mathbf{H}_{mn}^H \Phi_M \mathbf{h}_{t,k}^H = \sum_{m=1}^M \sum_{n=1}^N h_{rn}^* e^{-j\psi_n} H_{mn}^* e^{-j\eta_m} h_{t,k,m}^*,$$

$$\mathbf{h}_r^H \Phi_N \mathbf{H}_{m,n}^H \Phi_M \mathbf{h}_{t,k}^H = \sum_{m=1}^M \sum_{n=1}^N |h_{rn}| e^{-j\phi_{rn}} e^{-j\psi_n} |H_{mn}| e^{-j\phi_{mn}} e^{-j\eta_m} |h_{t,k,m}| e^{-j\phi_{t,k,m}},$$

$$\mathbf{h}_r^H \Phi_N \mathbf{H}_{mn}^H \Phi_M \mathbf{h}_{t,k}^H = \sum_{m=1}^M \sum_{n=1}^N |h_{t,k,m}| |H_{mn}| |h_{rn}| e^{-j(\phi_{t,k,m} + e^{-j\eta_m} + e^{-j\phi_{mn}} + e^{-j\psi_n} + \phi_{rn})},$$

$$\mathbf{h}_r^H \Phi_N \mathbf{H}_{mn}^H \Phi_M \mathbf{h}_{t,k}^H = \sum_{m=1}^M \sum_{n=1}^N |h_{t,k,m}| |\alpha_m| |H_{mn}| |\alpha_n| |h_{rn}| e^{-j(\phi_{t,k,m} + \eta_m + \phi_{mn} + \psi_n + \phi_{rn})},$$

- From the obtained result we can deduce that the total received signal power for each T_{x_k} at the R_x can be written as follows:

$$\begin{aligned}
P_{Rx}^k &= |\sqrt{L_{\tau,k}} e^{-j\Omega_3} \mathbf{h}_r^H \Phi_N \mathbf{H}_{mn}^H \Phi_M \mathbf{h}_{t,k}^H e^{-j\Omega_k}|^2 P_t, \\
&= |\sqrt{L_{\tau,k}} \sum_{m=1}^M \sum_{n=1}^N |h_{t,k,m}| |\alpha_m| |H_{mn}| |\alpha_n| |h_{rn}| e^{-j(\varphi_{t,k,m} + \eta_m + \varphi_{mn} + \psi_n + \varphi_{rn} + \Omega_k + \Omega_3)}|^2 P_t,
\end{aligned}$$

□